A Cadaveric and MRI Investigation of the Salpingopharyngeus

Karen Perta, MS, CCC-SLP

Purpose: To update our information regarding the salpingopharyngeus (SP) muscle using cadaveric and in vivo MRI data. Primary objectives were to a) observe the presence/absence of the muscle and b) quantify and describe its dimensions and course.

Method: Out of an original sample of 24 cadavers, 19 cadavers (10 females, 9 males), with a mean age at time of death of 77 years and weight at time of death of 156 pounds, were included in the analysis. Following head bisection, measurements of the SP, including width of the cartilaginous attachment (CW) and width of the superior muscle base (SMW), were taken before and after removal of the overlying mucosa. In addition, high resolution 3D MRI head scans from fourteen healthy participants (5 males, 9 females) were also analyzed. After identifying the opening to the Eustachian tube in a parasagittal image, CW and SMW measures were replicated in the axial MRI view.

Results: The presence of the salpingopharyngeal fold was confirmed bilaterally in all twenty-four cadavers, for a total of 48. Mean values of CW and SMW following mucosa removal were 5.6 mm and 3.8 mm, respectively. Results from a hierarchical regression analysis revealed that SMW is dependent on age and body weight at time of death, after controlling for sex. In the MRI data, the salpingopharyngeal fold and muscle were identified bilaterally in all 14 participants. Mean CW and SMW were 4.7 mm and 3.5 mm, respectively.

Conclusions: The salpingopharyngeal fold is always present, but its contents may be easily damaged or destroyed in the difficult dissection process. Though its inferior course is highly variable, the size of the SP muscle is dependent on cadaveric characteristics known to affect muscle fibers such as age and body weight. The salpingopharyngeal fold and muscle can also be identified in vivo using 3D MRI data. Given the consistent and quantifiable presence of the salpingopharyngeus, its potential role in velopharyngeal function for speech and swallowing are reconsidered.

Throughout the literature, there are highly variable reports regarding the presence, course, and function of the salpingopharyngeus (SP) muscle. The speech science literature has described SP as a small, sparse muscle of the nasopharynx that is not always present and has limited to no functional importance (Dickson & Dickson, 1972; Zemlin, 1998). In a landmark study, Dickson and Dickson (1972) found that in seven adult heads, the SP muscle was absent bilaterally in three specimens, present bilaterally in three specimens, and undetermined in one specimen. When present, the muscle was described as having “sparse” fibers originating from the palatopharyngeus (PP) and attaching to the torus tubarius. Furthermore, they reported the contents of salpingopharyngeal fold as mostly fibrous and glandular tissue, concluding that the SP is not always present and carries no functional significance. Similar information has been reiterated in speech science texts (Zemlin, 1998) and even reported in more recent cadaveric work (Choi et al., 2014). In contrast, older cadaveric speech science work suggested that SP may raise the velum to assist in velopharyngeal closure (Harrington, 1944). Current speech science texts (Seikel et al, 2009; Peterson-Falzone et al., 2010; Kummer, 2019) discuss the possibility of

the SP acting to elevate the lateral pharyngeal walls and open the Eustachian tube but deny its contribution to velopharyngeal closure.

In contrast, the anatomic literature reflects the consensus that the SP muscle acts with PP and stylopharyngeus to elevate the pharynx during swallowing, and the possibility of its absence is never acknowledged (Strandring, 2016; Norton, 2017; Baker, 2015). This information reflects other prior cadaveric studies that suggested the SP moves the lateral pharyngeal walls medially during speech and swallowing (Bosma, 1953; McMyn, 1940). For instance, in a study of six adult cadaver specimens, McMyn (1940) found that the SP was a small, muscular "slip" originating on the medial cartilaginous lamina of the eustachian tube (i.e. torus tubarius) and inserting into PP as well as the lateral and posterior pharyngeal walls. Though each specimen was unique in the size and course of its SP muscle, McMyn (1940) did not cite its absence in any of the specimens. Similarly, Bosma (1953) found in two of eight specimens, there were prominent muscle fibers originating at the cartilaginous portion of the eustachian tube and running inferiorly as "a band in the pharynx." In four of eight specimens, there were two distinct projections of the SP muscle – one from the medial cartilage projecting downward toward PP, and the other on the lateral portion of the cartilage coursing downward and medially into the lateral nasopharyngeal wall. However, in contrast to McMyn, Bosma noted the SP muscle to have "sparse fibers" that were not identifiable in the remaining two specimens. In general, both Bosma (1953) and McMyn (1940) found that SP commonly became continuous with PP inferiorly.

It is important to note that most prior cadaveric studies have used specimens preserved in a traditional-fix embalming solution that contains formaldehyde (Dickson & Dickson, 1972; Choi et al., 2014; Bosma, 1953); some studies do not provide specific preservation information

(Sumida et al., 2012; Harrington, 1944; McMyn, 1940). Though a common and relatively inexpensive preservation method, formaldehyde is known to cause stiffening, dehydration, and discoloration of cadaveric tissue, which poses challenges to dissection as well as surgical training (Hayashi et al, 2016). A more recent study of the SP muscle using fresh specimens reported the muscle present bilaterally in all 15 cadavers (Huang et al, 1997). Huang et al. (1997) found its superior attachment at both the cartilaginous and membranous portions of the medial eustachian tube and its inferior fibers continuous with PP at the level of the velum and lateral pharyngeal wall. However, they described the salpingopharyngeus as "vestigial" with a more fibrous rather than muscular composition, and thus concluded that the salpingopharyngeus could elevate the lateral pharyngeal wall but is unlikely to have functional importance. Of note, in addition to using fresh specimen, this study also reported sex, age and body weight at time of death (Huang et al, 1997), whereas this information has been mostly omitted from previous studies (Dickson & Dickson, 1972; Choi et al., 2014; Sumida et al, 2012; Bosma, 1953; Harrington, 1944; McMyn, 1940). As skeletal muscle is known to deteriorate with age and inactivity (McCormick & Vasilaki, 2018), these variables may account for some of the variation observed in cadaveric investigations. It is also important to note that no prior cadaveric studies have attempted to quantify the dimensions of the SP muscle.

In more recent decades, the use of magnetic resonance imaging (MRI) has gained popularity in providing quantitative structural and functional information regarding the velopharyngeal (VP) musculature. Many of these studies, conducted on living participants with and without cleft palate, have focused on in vivo measurements of the levator veli palatini (LVP) muscle because of its primary role in velar elevation for speech and swallowing (Ettema et al, 2002; Kuehn et al., 2004; Tian et al., 2010c; Bae et al., 2011; Perry et al., 2013, 2014). Based on

MRI data in normal individuals, average LVP thickness is approximately 5.4 mm (Ettema et al., 2002), and typical LVP length is 42.5 to 51.1 mm (Bae et al., 2011; Perry et al., 2014). The technological advancement from two-dimensional (2D) MRI to high resolution three-dimensional (3D) MRI has even allowed for quantification of the tensor veli palatini (TVP) muscle, which is approximately 2.5 mm in diameter and 3 mm in thickness (George et al., 2018). Despite its proximity to the LVP, TVP, and velum, there have been no previous MRI investigations of the SP muscle.

Perhaps due to the disputed presence/absence and function, as well as the highly variable size and course of the salpingopharyngeus, no quantitative data is available from either cadaveric or MRI sources. Thus, the purpose of this study was to update and quantify our information regarding SP using data from cadavers as well as high resolution 3D MRI in living participants. Based on information from the existing literature, we hypothesized that a) the salpingopharyngeal fold and muscle would be identifiable bilaterally in both cadaveric and MRI data b) the SP muscle size may be dependent on cadaveric characteristics, including sex, age, and body weight at time of death c) the SP would have a consistent superior origin at the torus tubarius but highly variable inferior course into the PP and/or pharyngeal wall and d) the width dimensions of the SP would be consistent across cadaveric and MRI measurement.

Method

Subjects

The study was approved by the Body Donor Program Advisory Committee at The Ohio State University. The original sample included twelve male and twelve female cadavers (age range: 57-90+ years). These specimens were shared with medical and dentistry students who were simultaneously completing other dissections. Due to inadvertent damage or removal of

nasopharyngeal structures, the final sample included 31/38 SP muscles from nineteen cadavers (10 females, 9 males) between 62 and 90+ years of age (mean: 77 years) with a body weight at time of death between 104 and 210 pounds (mean: 156 pounds). Seventeen cadavers were embalmed with a traditional formalin fix, and two specimens were preserved in an anatomical fix using a proprietary solution by Dodge chemicals.

The MRI portion of the study was accomplished via retrospective analysis of high-resolution 3D MRI data of the head obtained from prior studies with IRB approval. These healthy, normal participants were nine females and five males between 19 and 62 years of age (mean: 35 years). They all denied history of speech, voice or resonance pathology and illness at the time of scanning and passed an oral mechanism screening. For each participant, three-dimensional (3D) MRI data were collected at rest on a Siemens 3.0T scanner, using a SPACE (Sampling Perfection with Application Optimized Contrasts using different flip-angle Evolution) sequence with the following acquisition parameters: echo time (TE) = 354 ms, repetition time (TR) = 2500 ms, field of view (FOV): 256 × 256 × 208 mm^3, and acquisition matrix: 256 × 256 × 208 pixels. The 3D scan was approximately 4 minutes long.

Procedures and Measures

To access the salpingopharyngeus, the exact dissection approach included the following steps: 1) the head was bisected as close to the midsagittal plane as possible 2) the salpingopharyngeal fold was identified and palpated from the medial surface of the bisected head 3) using an electronic digital caliper (Neiko, model number 01407A), width measures were obtained with the overlying mucosa still intact 4) the overlying mucosa was carefully removed using hemostats and curved blunt/blunt scissors 5) width measures were repeated following mucosal removal. Head bisection was performed by medical and dentistry students. Mucosa

removal was completed by author KP with supervision and training from collaborator EK, an anatomist whose cumulative experience includes dissection of over 10,000 head specimens. The following measurements (in mm) were obtained from each side of a specimen: 1) width measurement across the thickest medial portion of the torus tubarius or cartilaginous attachment (i.e., cartilaginous width or CW) and 2) width measurement at the superior muscle attachment, just inferior to the point of cartilaginous attachment (i.e., superior muscle width or SMW). Width measures, determined based on visual inspection as well as manual palpation, were taken before and after removing the mucosa of the salpingopharyngeal fold (Figure 1). When obtaining the width measurements, the digital calipers were brought to the outer lateral margins of the specimen (i.e., mucosa or muscle) in order to avoid physical compression or alteration of the structure. Length measures were attempted; however, due to the highly variable inferior course of the SP muscle, a reliable and consistent definition for salpingopharyngeus length could not be obtained. Figure 2 demonstrates the varying lengths and points of inferior interdigitation of two different SP specimens following mucosa removal.

The SP measurements were obtained in vivo using a 3D visualization/processing software, Amira 5.6 (ThermoFisher Scientific, Hillsboro, OR). In-plane resolution was 1×1 mm for all MRI images included in the analysis. For enhanced visualization, all images used for measurements were post-processed using the Amira built-in interpolation algorithm (i.e., bilinear interpolation approach). The SP was visualized in the 3D MRI data by identifying the opening to the Eustachian tube in the parasagittal view. Next, an axial slice perpendicular to the course of the salpingopharyngeal fold was overlaid through the Eustachian tube (Figure 3). In the axial view, the slice was then moved superiorly and inferiorly in order to recreate width measures that were comparable to the cadaveric data. Cartilaginous width (CW) was taken from the axial plane

that bisected the vertical dimension of the cartilage (i.e., torus tubarius) at the medial portion (i.e., inferior to the superior curve). Superior muscle width (SMW) was obtained from the slice immediately inferior to the slice that contained the last visible pixel of the cartilage. Figures 4 and 5 depict CW and SMW measurements. Of note, due to the MRI image resolution (i.e., 1 mm^2), the overlying mucosa of the salpingopharyngeal fold could not be separated from the underlying muscle because the thickness of the mucosa is generally 1 mm or less. Thus, the MRI measures reflect the combination of both the mucosa and the muscle of the salpingopharyngeal fold and are most comparable to the cadaveric measures obtained prior to mucosa removal. Of note, the T2-weighted MRI images allowed for consistent identification of the underlying SP muscle as a homogenous region of gray pixels that can be readily distinguished from white areas of cartilage, adipose or glandular tissue and black areas that represent surrounding vessels or airspace. Indeed, T2 MRI imaging has been successfully used to evaluate muscle, cartilage, mucosa, and adipose tissue (i.e. Ostmann's fatty tissue) surrounding the Eustachian tube (Yoshida et al, 2018; Smith et al, 2016).

Reliability

Intraclass correlation coefficients were computed to determine the intrarater and interrater reliability of the cadaveric and MRI measures. In the cadaveric data, all CW and SMW measurements were obtained twice at two different time points to assess intrarater reliability. Mean differences between two sets of measurement were 0.1 mm (SD = .2) with an intraclass correlation coefficient that approximated 1 for both measures (ICC, 2-way mixed, absolute agreement, and single-measure). The second rater confirmed interrater reliability on 11/31 final salpingopharyngeal specimen, with mean differences of 0.2 mm (SD = .2) and an ICC coefficient of 0.94.

In the MRI data, all CW and SMW measurements were obtained twice at two different time points to assess intrarater reliability. For intrarater reliability, mean differences between two sets of measurements were ___ (SD =) with an ICC coefficient of ____. A third rater YB, a speech scientist with expertise in structural MRI analysis of the velopharyngeal mechanism, confirmed interrater reliability on all 28 MRI samples with mean differences of ___ (SD =) and an ICC coefficient of _____.

Statistical Analysis

A hierarchical regression analysis was performed to test the hypothesis that SMW, our dependent variable, would be dependent on cadaveric characteristics of sex, age and body weight (i.e., three independent variables). Age and body weight were centered at the mean (77 and 156, respectively). In block one, we examined the main effects of sex, body weight at time of death, and age on SMW. In block two, we included the interaction term of age by weight with the main effects to observe differential effects on SMW. For the statistical testing, SPSS version 26.0 software (IBM) was used with the α level set at .05.

Results

Cadaveric Data

Based on visual inspection, the salpingopharyngeal fold was confirmed present bilaterally in the initial sample of twenty-four cadaver specimens. There was one instance of an off-center head bisection, resulting in apparent damage to the left salpingopharyngeal fold from the saw cut. Thus, even though this sample could not be used for measurement, the salpingopharyngeal fold and its remaining contents could still be identified by gross visual inspection. It was determined that 48/48 salpingopharyngeal folds were present, but the final sample included 31/48 salpingopharyngeal folds due to other obvious unintentional specimen damage.

Descriptive statistics for CW and SMW before and after mucosa removal are summarized in Table 1. Mean CW values with (6.2 mm) and without mucosa (5.6 mm) differed from each other by .6 mm. Similarly, mean SMW values with (4.6 mm) and without mucosa (3.8 mm) differed from each other by .8 mm. Table 2 provides summary statistics of CW and SMW without mucosa for females and males separately. Both CW and SMW were greater in males than females with the mean CW values of 5.8 mm and 5.4 mm for males and females, respectively and the mean SMW values of 4.2 mm and 3.4 mm for males and females, respectively.

Results from the hierarchical regression analysis based on SMW data without mucosa revealed a significant main effect for sex (B = 1.1, p = .006). SMW was also found to be dependent upon the relationship between age and body weight at time of death after controlling for sex. Specifically, the effect of weight on SMW increased with the increase of age, and this interaction effect was statistically significant (B = .002, p =.04). The three main factors (sex, body weight, and age) and the interaction term (age by body weight) explained 38% of the variance in SMW (F = 3.958, p = .012). However, when the same hierarchical regression was performed using CW (i.e., without mucosa) as the dependent variable, the model was nonsignificant (F = .606, p = .617) without any significant main effects or interactions (i.e. age by body weight). The hierarchical regression models are summarized in Tables 3 and 4.

MRI Data

In the MRI data, the 1 mm^2 image resolution did not allow separation of the SP muscle and mucosa; thus, these measurements are most similar to cadaveric measured conducted prior to mucosa removal. However, the salpingopharyngeal fold and its contents were consistently identified bilaterally in all fourteen living participants, for a total of 28. Sample average CW and

SMW were 4.7 mm and 3.5 mm, respectively. Descriptive statistics by sex are summarized in Table 5.

Discussion

The present study successfully utilized cadaveric and MRI data to investigate and quantify the salpingopharyngeus using width measures along the superior muscle base (SMW) as well as its cartilaginous origin (CW). Our findings support the first hypothesis that the salpingopharyngeal fold and muscle would be identifiable bilaterally in both the cadaver and living participants. Thus, results of this study provide updated information regarding SP and aim to clarify the discrepancies found across the literature.

Perhaps the most salient reason for discrepancy in the presence/absence of the salpingopharyngeus is the inherent intricacy and complexity of the dissection itself. Several different dissection approaches have been employed across the literature, likely because the muscles of the nasopharynx are so difficult to access. For example, the initial work by Dickson & Dickson (1972) utilized head bisection followed by medial and lateral approaches for 5/7 specimens as well as lateral and posterior approaches with an intact head for 2/7 specimens. A similar variety of dissection approaches was also employed by Sumida and colleagues (2017). As we found in our approach, the salpingopharyngeal fold can be disturbed if the initial saw cut to bisect the head is not precisely midsagittal. However, other posterior and/or lateral approaches that do not involve head bisection would complicate physical access to the salpingopharyngeal fold, as it would be nearly impossible to insert digital calipers along its supero-medial origin. Once the entire salpingopharyngeal fold can be visualized from the superior origin near the Eustachian tube opening (i.e. torus tubarius) along its inferior course into the pharynx, then the overlying mucosa must be carefully removed in order to inspect its contents. Our finding is that

the mucosa itself is often 1 mm or less in thickness (see Figure 1, Middle) and is challenging to remove without disturbing underlying muscle fibers, especially in the traditional-fix specimens with stiffened and dehydrated tissues (Hayashi et al, 2016). These inherent difficulties, in addition to sharing our cadaveric sample with students who were simultaneously conducting other dissections for medical and dentistry training, ultimately reduced our original sample of 48 down to 31 useable salpingopharyngeal folds. The fact that we experienced an inadvertent reduction in sample size does not mean the structures were not originally present and intact.

Another possible explanation for the reports of salpingopharyngeus absence in cadaveric work pertains to our third hypothesis regarding its relatively consistent origin but highly variable course to its insertion. It is well-established that SP originates superiorly at the torus tubarius but has a highly variable inferior course, often becoming continuous with the PP muscle as well as the pharyngeal wall (McMyn, 1940; Huang et al, 1997; Sumida et al, 2012; Standring, 2016). Thus, we hypothesized that SP would have a consistent superior origin at the torus tubarius but highly variable inferior interdigitation with PP and/or pharyngeal wall. In a recent cadaveric study, Choi and colleagues (2014) reported SP present in only 63.6% of cases. It should be noted that their dissection approach involved separating the pharynx from the skull base, which included only the pharyngeal opening to the auditory canal (i.e., membranous Eustachian tube). As the cartilaginous portion of the Eustachian tube (i.e. torus tubarius), the origin of the SP, is anchored to the cranial base, this superior section of SP would likely have been removed from the analysis, as can be seen in similar images provided by Sumida and colleagues (2012). Indeed, their region of interest included the longitudinal pharyngeal muscles at the oropharyngeal and laryngeal levels (i.e., lateral to the thyroid cartilage), where the SP muscle was reported absent (Choi et al, 2014). For this same reason, we had difficulty developing a consistent measurement

definition for SP length, as this feature is highly variable across individuals. For instance, cases of a long SP may interdigitate with PP and pharyngeal constrictors at the oropharyngeal or even laryngopharyngeal level, whereas cases of a short SP may dive into PP at the level of the velum and the pharyngeal wall at the level of the superior pharyngeal constrictor (see Figure 2). It is important to note that the latter cases would show an absence of SP muscle fibers at the more inferior oropharyngeal or laryngopharyngeal level – but not necessarily at its superior origin. Hence, both our cadaver and MRI data show that SP is consistently present at its superior origin at the torus tubarius, despite having a highly variable inferior course.

Finally, an additional explanation for the variable reports across cadaveric literature relates to our second hypothesis that SP muscle size may be dependent on cadaveric characteristics, including sex, age, and body weight at time of death. Indeed, our regression analysis results showed that SP muscle size (i.e. SMW) is affected by sex as well as the relationship between age and body weight at time of death with the sex variable controlled. However, this was not true for the width across the cartilaginous origin of SP (i.e., CW at the torus tubarius). It is well-known that cartilage does not respond to age-related changes (i.e., atrophy) and load-bearing activity (i.e., exercise) in the same manner as muscle fibers, with cartilage being much less susceptible to age and activity-induced changes (McCormick & Vasilaki, 2018; Eckstein et al, 2006). Of note, it has been reported that in traditional-fix specimens, the muscle fiber content of the salpingopharyngeal fold is often replaced by connective and/or adipose tissue (Sumida et al, 2011; Sumida et al, 2017). Similarly, in fresh specimens, Huang and colleagues (1997) reported that the contents of the salpingopharyngeal fold are occasionally more fibrous rather than muscular. However, it has been difficult to determine if these findings are simply the result of the death process or also the case for living individuals. Our MRI data suggest that muscle fiber is

consistently present in living individuals, as evidenced by homogenous areas of gray pixel on the T2-weighted images (see Figure 5) that appear distinct from bright white areas of cartilage, adipose, and/or glandular tissue as well as black areas of vessel and/or airspace. Indeed, prior MRI investigation of the Eustachian tube and surrounding structures has successfully used T2-weighted images to delineate TVP muscle fiber from Eustachian tube opening from Ostmann's fatty tissue (Yoshida et al, 2018). Thus, we conclude that while SP muscle size appears to be dependent on specific characteristics of the cadaver specimens such as sex, age, and body weight at time of death, this may or may not be true in the living. Such variables should be considered and consistently reported in future cadaveric studies.

Our findings partially support the last hypothesis that the width dimensions of the SP muscle base (SMW) and cartilaginous attachment (CW) would be consistent across cadaveric and MRI measurement. To the best of our knowledge, our study is the first to report measures of SP using in vivo MRI. Previous MRI investigations of the surrounding structures of the Eustachian tube, conducted using 2D scans and lower image resolution, have not included the salpingopharyngeus (Yoshida et al, 2018). As previously stated, MRI width measures at the level of the cartilage (CW) and superior muscle base (SMW) are most comparable to cadaveric measures before mucosal removal. The sample means for CW and SMW were 6.2 mm and 4.6 mm for the cadaver data versus 4.7 mm and 3.5 mm for the MRI data. The smaller overall values in the MRI data were somewhat unexpected findings that may have a few explanations. First, while taking cadaveric width measures, caution was taken to avoid obvious physical compression of the specimen between the digital calipers. Though these measures are supported by strong interrater and intrarater reliability, this measurement approach may have resulted in slightly inflated values. Also, the 1 mm^2 isotropic resolution in the MRI data, relative to a

structure that is approximately 3.5 mm wide, may have further contributed to measurement error as well as discrepancy with the cadaveric data. Indeed, though MRI data has previously established LVP muscle thickness of 3.9 to 5.4 mm (e.g., Ettema et al., 2002), cadaveric data has also reported slightly larger LVP diameters of 7.4 to 8.6 mm (e.g., Huang et al, 1997). Our data demonstrate a similar pattern when quantifying SP. Therefore, differences between cadaveric and MRI data may be explained by inherent limitations in their respective measurement approaches.

In addition to providing further clarification regarding salpingopharyngeus presence, size, and course, our data also raise a few questions. If the SP muscle is consistently present in the living, but its course is highly variable, then what does this imply about its possible function? While several actions (and inactions) have been ascribed to SP, including limited to no importance/function (Dickson & Dickson, 1972; Huang et al, 1997), possible downward pull on the Eustachian tube (Dickson & Dickson, 1972), elevating the pharyngeal walls (McMyn, 1940, Bosma, 1953; Kummer, 2019; Standring, 2016), and elevating the velum (Harrington, 1944), it is difficult to draw such conclusions based on cadaveric data alone. However, it is doubtful that the salpingopharyngeus, with its narrow width of approximately 3.5 mm and variable inferior course, is able to generate the muscular force required to move cartilage (i.e., torus tubarius) that is anchored to the cranial base. Based on its size and structure, it seems more likely that the salpingopharyngeus exerts an upward pull on the structures of its inferior interdigitation, including PP and the pharyngeal walls, approximating them toward the point of origin at the torus tubarius. Interestingly, Chien and colleagues (2007) provide a case report regarding Botox injections for treatment of palatal tremor. In this example, Botox injections into both SP and PP were maximally effective for treating ear click symptoms related to palatal tremor, whereas prior

injections into the TVP or SP alone had minimal efficacy in reducing palatal tremor and ear clicking symptoms (Chien et al, 2007). Though the authors attribute the treatment efficacy to the role of SP in Eustachian tube opening, it is unclear if the clinical results are specific to the location of the injections (i.e., TVP versus SP versus PP) or the fact the injections were repeated several times with additional dosing. It is also important to note that the injections into both the SP and PP resulted in maximal reduction of palatal tremor and its associated ear clicking symptom. As a result, this case may in fact illustrate that SP has more influence on velar movement, rather than the Eustachian tube, via its direct relationship to PP.

Furthermore, despite reporting the salpingopharyngeus inconsistently present, Sumida and colleagues (2017) have reported detailed cadaveric findings regarding the palatopharyngeal sphincter (PPS). These authors explain that the PPS, a band of transverse muscle fiber that runs along the medial aspect of the superior pharyngeal constrictor (SPC), is responsible for the formation of Passavant's ridge that enhances nasopharyngeal closure by cinching the superior nasopharynx (i.e., SPC) and drawing the salpingopharyngeal fold toward the velum (Sumida et al, 2017). This action could potentially occur in speech or swallowing. In contrast, a previous MRI and endoscopic investigation described medialization of the pharyngeal walls during VP closure for speech tasks, but the authors attributed this action to contraction of the LVP and fail to mention possible contributions from PPS or SP (Yamawaki et al, 1999). Prior electrophysiologic (e.g., EMG) data, obtained in vivo with normal individuals as well as participants with and without repaired cleft palate, have documented palatopharyngeal activity during swallowing but not speech (Trigos et al, 1988). In contrast, other prior EMG data has shown palatopharyngeal activity for velar positioning during speech production tasks using oral consonants, but these studies did not comment on the salpingopharyngeus (Seaver & Kuehn,

1980; Bell-Berti, 1976). Trigos and colleagues (1988) reported SP activity in only 20-40% of subjects, but the insertion of a single needle (into a somewhat ambiguous location on the posterior faucial arch) makes distinction between true palatopharyngeal and salpingopharyngeal activity difficult. In addition, due to individual variability in some participants, the salpingopharyngeal muscle may have already interdigitated at a location more superior to the needle placement. The role of the palatopharyngeus in swallowing is well-established, but it is also known to affect velar movement (Choi et al, 2014; Norton, 2017; Standring, 2016; Baker, 2015). Based on prior EMG data (Trigos et al, 1988; Seaver & Kuehn, 1980; Bell-Berti, 1976), it is still reasonable to conclude that speech and swallowing tasks require various degrees of nasopharyngeal closure with differences in the activity of associated muscles. Velopharyngeal closure may be accomplished by both velar movement in the superior and posterior dimensions, via LVP and transverse fibers of PP respectively, as well as simultaneous movement of the superior pharynx in the anterior dimension via PPS and/or SP. Our findings suggest that because the salpingopharyngeus is a consistently present component of the posterior nasopharyngeal mechanism, it may potentially contribute to velopharyngeal closing actions required by living individuals for speech and/or swallowing.

Conclusion

This was the first study to successfully utilize both cadaveric and MRI data to investigate and quantify the salpingopharyngeal fold and muscle. Our findings further explain the prevalence of the salpingopharyngeus, which is always present at its superior origin at the torus tubarius but has a highly variable inferior interdigitation with palatopharyngeus and pharyngeal constrictors. Due to significant individual variation, its inferior insertion points can be found anywhere between the level of the velum and superior pharyngeal constrictor and the level of the

inferior pharyngeal constrictor and supero-lateral aspect of the larynx (i.e., near the epiglottis or thyroid cartilage). Variability in cadaveric reports may be further explained by variations in dissection approach and preservation methods as well as cadaveric characteristics such as sex, body weight, and age. Along the intact cadaveric salpingopharyngeal fold, average widths across the cartilaginous attachment (CW) and superior muscle (SMW) are approximately 6.2 mm and 4.2 mm, respectively. These values are in slight contrast to in vivo MRI data that reveal smaller averages of 4.7 mm and 3.5 mm for CW and SMW, respectively.

There are several limitations to this study. First, the damage to 17/48 salpingopharyngeus specimen, though unintentional, was unfortunate. Also, the use of a dissecting microscope as well as staining techniques would have increased the quality and accuracy of the dissection and identification of muscle fibers. A greater number of living participants as well as the inclusion of body weight information would have allowed for further statistical analysis in the MRI data. As previously discussed, there are also inherent limitations in both cadaveric and MRI measurement. Visual inspection and measurement with digital calipers may provide slightly inflated values, whereas MRI analysis with 1 mm^2 isotropic resolution may provide slightly conservative measures that are subject to a proportionally higher margin of error (i.e., 1 mm resolution to a 3.5 mm muscle) despite strong measures of interrater and intrarater reliability. Though MRI images can provide an accurate depiction of a muscle from origin to insertion and allow for delineation from surrounding structures such as cartilage or adipose tissue, histologic tissue sampling would be the only way to truly confirm that the contents of the living salpingopharyngeal fold include muscular rather than fibrous composition.

Future studies may include an increased number of both cadaveric and living participants. Though the use of traditional-fix cadavers is much more common, the anatomical fix or even fresh specimen may be more conducive to mucosa removal for purposes of studying the salpingopharyngeal fold and underlying muscle. Also, future MRI studies of the velopharyngeal mechanism may incorporate analysis of the salpingopharyngeus, especially as this becomes more feasible with advances in MRI technology. Future study of salpingopharyngeal activity during speech and swallowing may require further improvement in real-time MRI techniques, which currently involve lower spatial and temporal resolution that may be insufficient for analysis.

Increasing the quantitative information regarding velopharyngeal musculature is ultimately important for our understanding of VP anatomy and physiology in both normal and disordered populations. Accurate information is essential for informing clinical treatment as well as surgical approaches in populations with abnormal VP structure and/or function. Future studies may aim to investigate all major structures of the VP mechanism, including the salpingopharyngeus.

Acknowledgements

The author would like to thank the Body Donor Program at The Ohio State University for the ability to complete the study. Also, thank you to Dr. Eileen Kalmar and Dr. Youkyung Bae for support and assistance with inter-rater reliability measurements.

References

Bae, Y., Kuehn, D.P., Sutton, B.P., Conway, C.A., & Perry, J.L. (2011). Three-dimensional magnetic resonance imaging of velopharyngeal structures. *Journal of Speech Language and Hearing Research, 54,*1538-1545.

Baker, E. (2015). *Anatomy for Dental Medicine.* 2nd ed. New York, NY: Thieme Medical Publishers, Inc.

Bell-Berti, F. (1976). An electromyographic study of velopharyngeal function in speech. *Journal of Speech and Hearing Research, 19,* 225-240.

Bosma, J. (1953). A correlated study of the anatomy and motor activity of the upper pharynx by cadaver dissection and by cinematic study of patients after maxilla-facial surgery. *Annals of Otology, Rhinology, & Laryngology, 62 (1),* 51-72.

Chien, H.F., Sanchez, T.G., Sennes, L.U., & Barbosa, E.R. (2007). Endonasal approach of salpingopharyngeus muscle for the treatment of ear click related to palatal tremor. *Parkinsonism and Related Disorders, 13,* 254-256.

Dickson, D. & Dickson, W. (1972). Velopharyngeal anatomy. *Journal of Speech, Language, and Hearing Research, 15(2),* 372-381.

Eckstein, F., Hudelmaier, M., & Putz, R. (2006). The effects of exercise on human articular cartilage. *Journal of Anatomy, 208(4),* 491-512.

Ettema, S.L., Kuehn, D.P., Perlman, A.L., Alperin, N. (2002). Magnetic resonance imaging of the levator veli palatini muscle during speech. *Cleft Palate Craniofacial Journal, 39,*130-144.

George, T., Kotlarek, K., Kuehn, D., Sutton, B., & Perry, J. (2018). Differences in the tensor veli palatini between adults with and without cleft palate using high-resolution 3-dimensional magnetic resonance imaging. *The Cleft Palate-Craniofacial Journal, 55(6),* 697-705.

Harrington, R. (1944). A study of the mechanism of velopharyngeal closure. *Journal of Speech and Hearing Disorders, 9 (4),* 325-345.

Hayashi, S., Naito, M., Kawata, S., Qu, N., Hatayama, N., Hiari, S., & Itoh, M. (2016). History and future of human cadaver preservation for surgical training: from formalin to saturated salt solution method. *Anatomy Science International, 91(1),* 1-7.

Huang, M.H.S., Lee, S.T., & Rajendran, K. (1997). A fresh cadaveric study of the paratubal muscles: Implications for eustachian tube function in cleft palate. *Plastic and Reconstructive Surgery, 100 (4),* 833-842.

Kuehn, D.P., Ettema, S.L., Goldwasser, M.S., & Barkmeier, J.C. (2004). Magnetic resonance imaging of the levator veli palatini muscle before and after primary palatoplasty. *Cleft Palate Craniofacial Journal, 41,* 584-592.

Kummer, A.W. (2019). *Cleft Palate and Craniofacial Conditions: A Comprehensive Guide to Clinical Management*. 4th ed. Burlington, MA: Jones and Bartlett Learning.

McCormick, R. & Vasilaki, A. (2018). Age-related changes to skeletal muscle: changes to lifestyle as a therapy. *Biogerontology, 19(6),* 519-536.

McMyn, J.K. (1940). The anatomy of the salpingopharyngeus muscle. *Journal of Laryngology and Otology, 55 (1),* 1-22.

Norton, N. (2017). *Netter's Head and Neck Anatomy for Dentistry*. 3rd ed. Philadelphia, PA: Elsevier, Inc.

Perry, J.L., Kuehn, D.P., & Sutton, B.P. (2013). Morphology of the levator veli palatini muscle using magnetic resonance imaging. *The Cleft Palate-Craniofacial Journal, 50,* 64-75.

Perry, J.L., Kuehn, D.P., Sutton, B.P., & Gamage, J.K. (2014) Sexual dimorphism of the levator veli palatini muscle: an imaging study. *The Cleft Palate-Craniofacial Journal, 51,* 544-552.

Peterson-Falzone S., Hardin-Jones, M., & Karnell, M. (2010). *Cleft Palate Speech.* 4th ed. St. Louis, MO: Mosby Elsevier.

Seaver, E. & Kuehn, D. (1980). A cineradiographic and electromyographic investigation of velar positions in non-nasal speech. *The Cleft Palate Journal, 17(3),* 216-226.

Seikel, J.A., King, D.W., & Drumright, D.G. (2009). *Anatomy & Physiology for Speech, Language, and Hearing.* 4th ed. Clifton Park, NY: Delmar Cengage Learning.

Smith, M.E., Scoffings, D.J., & Tysome, J.R. (2016). Imaging of the Eustachian tube and its function: a systematic review. *Neuroradiology, 58,* 543-556.

Standring, S. (2016). *Gray's Anatomy: The Anatomical Basis of Clinical Practice.* 41st ed. New York, NY: Elsevier Limited.

Sumida, K, Yamashita, K, & Kitamura, S. (2012). Gross anatomical study of the human palatopharyngeus muscle throughout its entire course from origin to insertion. *Clinical Anatomy, 25(3),* 314-323.

Sumida, K., Ando, Y., Seki, S., Yamashita, K., Fujimura, A., Baba, O., Kitamura, S. (2017). Anatomical status of the human palatopharyngeal sphincter and its functional implications. *Surgical and Radiologic Anatomy, 39 (11),* 1191-1201.

Tian, W., Yin, H., Redett, R.J., Shi, B., Shi, J., Zhang, R., & Zheng, Q. (2010c). Magnetic resonance imaging assessment of the velopharyngeal mechanism at rest and during speech in Chinese adults and children. *Journal of Speech Language and Hearing Research, 53,* 1595-1615.

Trigos, I., Ysunza, A., Vargas, D., & Del Carmen Vazquez, M. (1988). The san venero roselli pharyngoplasty: An electromyographic study of the palatopharyngeal muscle. *Cleft Palate Journal, 25 (4),* 385- 388.

Yamawaki, Y., Nishimura, Y., & Suzuki, Y. (1999). Eustachian tube cartilage and medial movement of lateral pharyngeal wall on phonation. *Plastic and Reconstructive Surgery, 104 (2),* 350-356.

Yoshida, H., Takahashi, H., & Morikawa, M. (2018). Anatomy of the surrounding tissue of the eustachian tube in patulous eustachian tube: 3 tesla magnetic resonance imaging approach. *Otology & Neurology, 40,* e107-e114.

Zemlin, W.R. *Speech and Hearing Science: Anatomy and Physiology.* 4th ed. Boston, MA: Allyn & Bacon, 1998.

Table 1.

Descriptive statistics for cartilaginous width (CW) and superior muscle width (SMW) in cadaveric data.

	Mucosa			No Mucosa		
	Mean	SD	Range	Mean	SD	Range
CW (mm)	6.2	1.0	4.2-8.0	5.6	0.9	3.8-7.1
SMW (mm)	4.6	0.99	2.9-6.5	3.8	1.0	2.1-5.8

Table 2.

Descriptive statistics for cartilaginous width (CW) and superior muscle width (SMW) without mucosa in cadaveric data by sex.

	Male			Female		
	Mean	SD	Range	Mean	SD	Range
CW (mm)	5.8	0.7	4.2-6.7	5.4	0.9	3.8-7.1
SMW (mm)	4.2	0.9	2.3-5.3	3.4	1.0	2.1-5.8

Table 3.

Summary of hierarchical regression analysis for variables predicting superior muscle width (SMW) without mucosa in mm (N=31)

	Block 1			Block 2		
Variable	B	SE B	β	B	SE B	β
Sex	1.208*	.395	.594*	1.111**	.373	.546**
Body weight	-.013	.006	-.392	-.016*	.006	-.479*
Age	-.016	.021	-.130	-.026	.020	-.204
Age x Body weight				.002*	.001	.364*
R^2		.266			.378	

Note: Age and body weight were centered at their means

*$p < .05$. **$p < .01$.

Table 4.

Summary of hierarchical regression analysis for variables predicting cartilaginous width (CW) without mucosa in mm (N=31)

	Block 1			Block 2		
Variable	B	SE B	β	B	SE B	β
Sex	.483	.372	.285	.427	.371	.251
Body weight	-.003	.006	-.101	-.005	.006	-.162
Age	-.008	.020	-.074	-.013	.020	-.126
Age x Body weight				.001	.001	.255
R^2		.063			.118	

Note: Age and body weight were centered at their means

*$p < .05$. **$p < .01$.

Table 5.

Descriptive statistics for cartilaginous width (CW) and superior muscle width (SMW) in MRI data by sex.

	Male				Female			
	N	Mean	SD	Range	Mean	*N*	SD	Range
CW (mm)	5	4.6	0.7	3.7-6.6	4.8	9	0.6	4.1-6.1
SMW (mm)	5	3.3	0.5	2.6-4.1	3.5	9	0.6	2.5-4.7

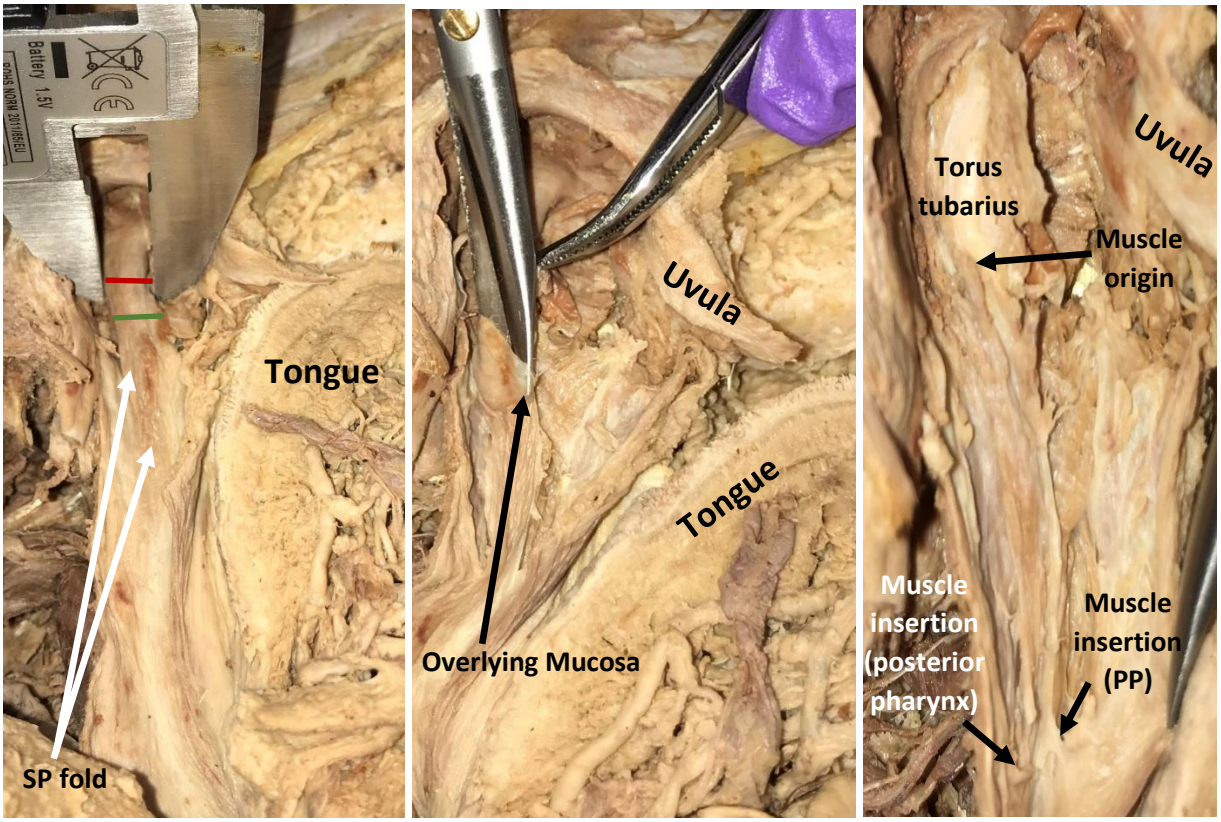

Figure 1.

Left: Cadaveric width measures with digital calipers, before mucosa removal. The red line represents approximate cartilaginous width (CW) and the green line represents approximate superior muscle width (SMW).

Middle: Dissection process of removing the overlying mucosa.

Right: The salpingopharyngeus from its origin to common insertion points, mucosa removed.

*SP = salpingopharyngeal *PP= palatopharyngeus

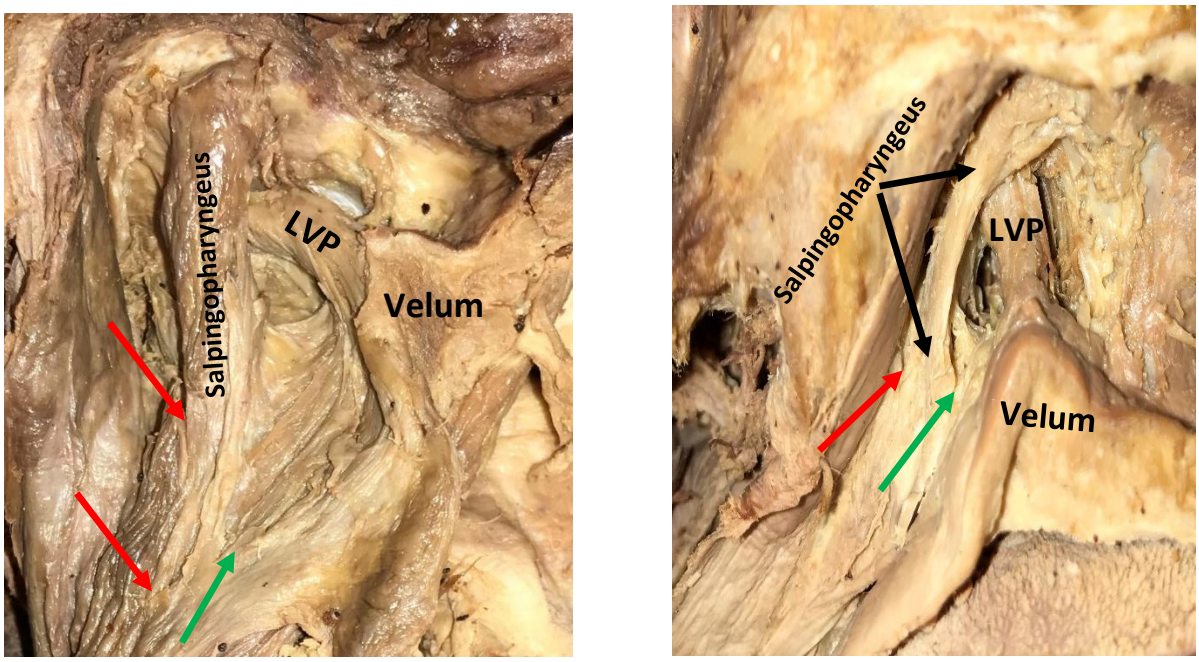

Figure 2.

Left-sided salpingopharyngeus muscles from two different cadaver specimen (both female), mucosa removed. Note the variation in size as well as inferior points of interdigitation.

LVP = levator veli palatini

Red arrows = points of salpingopharyngeus interdigitation with the pharyngeal wall

Green arrows = points of salpingopharyngeus interdigitation with the palatopharyngeus

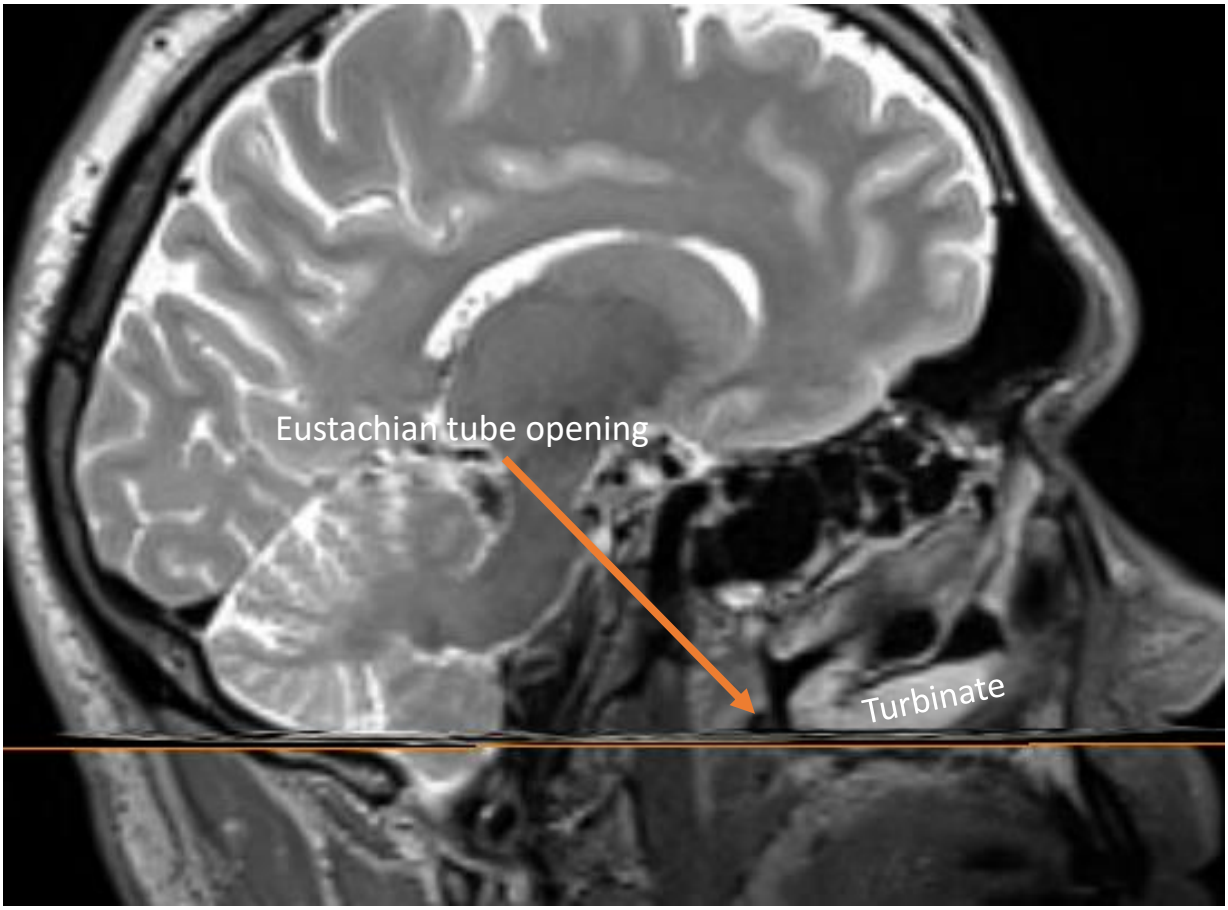

Figure 3.

An MRI parasagittal view with overlaid axial slice through the Eustachian tube opening, from the anterior nasal spine along the inferior margin of the posterior cerebellum.

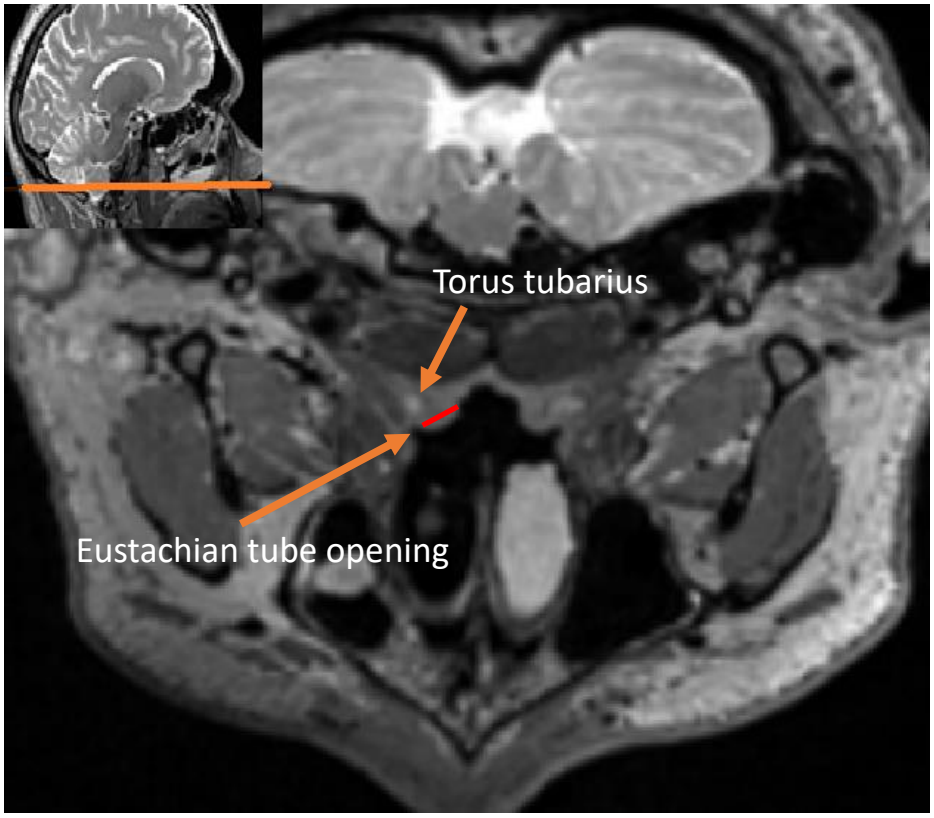

Figure 4.

An MRI axial view at the level of the cartilaginous width (CW – red line).

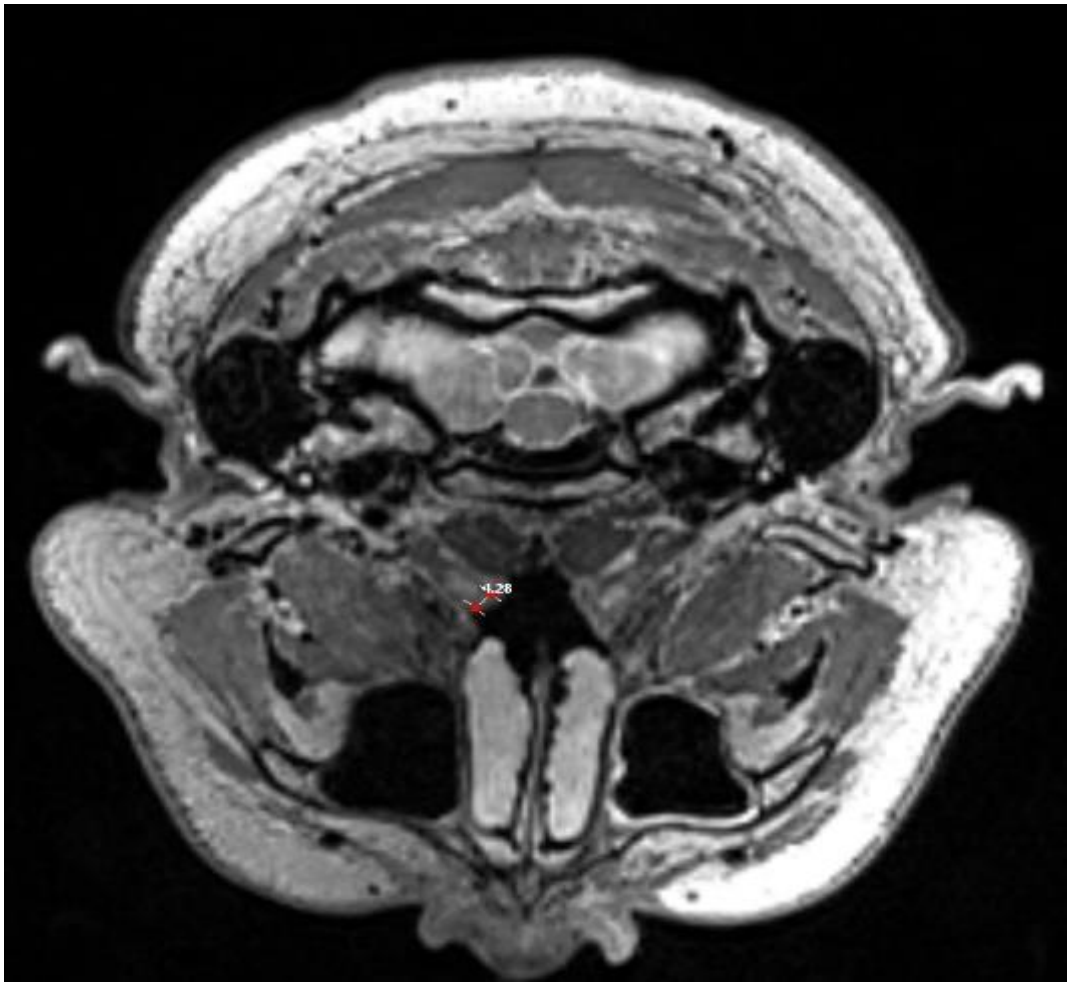

Figure 5.

An MRI axial view at the level of the superior muscle width (CMW – green line). Note this slice is at an inferior level relative to Figure 4.